

Experimental study of laminar film condensation on horizontal and vertical cylinders with Stefan number greater than unity

R. K. Sharma sharmar@colorado.edu
R. L. Mahajan mahajan@colorado.edu
Department of Mechanical Engineering
University of Colorado at Boulder, CO-80309-0427, USA

Abstract. *In this paper, we report first ever-experimental data for laminar condensation heat transfer on horizontal and vertical cylinders for fluids with Stefan number greater than unity. The condensation experiments were carried out in saturated vapor of FC5311[®] with ¼” and ½” diameter copper cylinders for aspect ratios (L/D) ranging from 1 to 32. In our first set of experiments, lumped capacity method was used to determine the heat transfer coefficients. Benchmarking experiments for spheres matched with those reported in literature. Our results for horizontal cylinder indicate that for large aspect ratios (>16) condensation heat transfer coefficients were close to those predicted by Nusselt correlation for horizontal circular cylinders. With decrease in aspect ratio, the heat transfer rate increased due to contribution from cross flow and the sides. A correlation incorporating the effect of aspect ratio is presented. For vertical cylinders, condensation heat transfer for high aspect ratio (>8) was higher than that predicted by Nusselt correlation. This was attributed to the onset of waviness in the condensate film. At low aspect ratios, however, heat transfer in vertical cylinders was lower than the predicted values due to condensate run-off from the top horizontal surface. These results will contribute towards improved condenser design for applications, such as vapor phase condensation soldering process, deploying such liquids.*

Keywords: *condensation heat transfer, Stefan number, finite cylinders*

1. Introduction.

The classical analysis of film condensation heat transfer on vertical flat surfaces and horizontal tubes is due to Nusselt (1916). Assuming linear temperature profiles, neglecting convective and inertia effects, the local heat transfer rate, Nu_x , was derived:

$$Nu_x = \left[\frac{(\rho_l - \rho_g) g h_{fg} x^3}{4 \nu_l k (T_{sat} - T_w)} \right]^{1/4} \quad (1)$$

where ρ_b , h_{fg} , ν_b , k , ρ_g , g , x , T_{sat} and T_w denote density, latent heat of vaporization, kinematic viscosity and thermal conductivity of the condensate, vapor density, acceleration due to gravity, characteristic length, saturation temperature of the vapor and wall temperature of the

cooling surface, respectively. Several researchers have extended and modified the analysis since then. Notable among these are Bromley (1952), Rohsenow (1956), Sparrow and Gregg (1959), Sparrow and Siegel (1959), Koh *et al.* (1961), Chen (1961), Dhir and Leinhard (1971). Selin (1961), Gerstmann and Griffith (1967) and Leppert and Nimmo (1968) have developed approximate correlations for condensation on inclined tubes, on underside of inclined flat surfaces and on top of finite horizontal surfaces, respectively. Merte (1973) has provided a comprehensive review of these and other earlier results.

Dhir (1975) proposed that steady state solutions were valid in quasi-steady condensation (Sparrow and Siegel, 1959) as long as the dimensionless thermal diffusion time constant is small and the film is not sluggish. Bejan (1991) considered the effect of run-off from the horizontal top surface for finite vertical cylinders and vertical slabs. Shigechi *et al.* (1993) developed a two-dimensional analysis to predict laminar film condensation heat transfer rates on finite horizontal plates facing upwards.

However, most of the studies of condensation heat transfer discussed above are for relatively small sensible heat effects for fluids with Stefan numbers less than unity. In the last couple of decades, a new family of Fluorinert fluids with high Stefan numbers has gained prominence due to application in various industries for condensation soldering (Chu *et al.*, 1974; Pfahl *et al.*, 1975; Wenger and Mahajan, 1979a, 1979b, 1979c). It involves immersing articles with pre-deposited solder in a body of saturated Fluorinert fluid vapor. The basic soldering machine is very similar to the experimental chamber shown in Fig. 1. Since the vapor is much heavier than air, a stable body of saturated vapor can be maintained in the vessel between the boiling fluid and the condensing coils. The only experimental study to-date, dealing specifically with fluids with Stefan number greater than unity is due to Mahajan *et al.* (1991). By conducting laminar film condensation experiments on copper spheres with Fluorinert fluid FC-70, it was shown that for these large Prandtl number and high Stefan number fluids, the Nusselt-Rohsenow expression is an accurate predictor, which is Eq. (1) with h_{fg} replaced by h_{fg}' where h_{fg}' is $(1+0.68S)h_{fg}$ and $S(=Cp(\Delta T)/h_{fg})$ is the Stefan number, is an accurate predictor. The heat transfer rates were calculated based on quasi-steady temperature response of the spheres. The deviations from theoretical values were lower (~10%) at higher values of S and higher at lower S . This was attributed to non-condensable components that became increasingly larger as surface temperature approached saturation temperature.

Although the above quoted study by Mahajan *et al.* (1991) broke some ground in obtaining experimental data for condensation of these fluids on spheres, no comparable study has been carried out for vertical and horizontal cylinders. The end effects in finite horizontal cylinders and the influence of condensation from the top and bottom surfaces on vertical cylinders have not been investigated. The present study was undertaken to fill the knowledge gap identified above. In part I of this study, we present our results on laminar film condensation of Fluorinert fluid FC5311[®] on cylinders with different aspect ratios in horizontal and vertical configurations.

2. Experiment

2.1. Fluid Properties

The condensing fluid used in the present investigation is FC5311[®], a perfluoro-perhydrophenanthrene, a member of the perfluorinated inert fluids manufactured by 3M. The relevant physical properties of this fluid at 25°C, taken from the 3M Fluorinert Electronic Liquid Product Manual, are given in Table 1. The property variations were calculated from the temperature-based relations indicated by Mahajan *et al.* (1991).

Table 1 Physical Properties of FC5311®

| | |
|--|---------------------|
| Typical boiling point, °C | 215 |
| Surface Tension, N/m | 19×10^{-3} |
| Heat of Vaporization, kJ/kg | 67.76 |
| Density, kg/m ³ | 2030 |
| Kinematic Viscosity, m ² /s | 14×10^{-6} |
| Specific Heat, kJ/kg.K | 1.05 |
| Thermal Conductivity, W/m | .055 |

2.2 Quasi-Steady State Experiments

The experimental apparatus, as shown in Fig. 1, consists of an insulated Pyrex jar, 305mm in diameter and 600mm in height, fitted with a 1.5kW immersion heater at the bottom and 6mm OD cooling water coils at the top. The electric immersion heaters were used to boil the liquid at the base of the jar while the water-cooled coils at the top were used to condense the vapor. Since this vapor is ~27 times heavier than air, a stable stratified saturated vapor region can be maintained in steady state between the cooling coils and the top of the boiling liquid. The space above this region of saturated vapor was filled with air. Power input to the heaters was controlled using a variac. The jar was fitted with a stainless steel cover, with a smaller removable cover to allow the specimens to be inserted. A thermocouple probe was kept inserted inside the jar during the experiment to record the saturation temperature of the vapor.

Each copper specimen was supported from bottom by a stainless steel tube to prevent the flow of condensate from the tube to specimen. A ceramic sleeve was used to attach the stainless steel tube to the copper coupon to prevent heat loss due to conduction. Thermocouples used to measure the specimen temperatures were positioned at the geometric center of each specimen, with the leads running through the ceramic tube and the stainless steel tube. Thermal grease was used to provide a sound thermal contact between the specimen and the thermocouple bead. They were held together by the weight of the specimen itself. Figure 2 shows the cross-section detail of the thermocouple attachment with the specimen and Table 2 provides the physical dimensions and weights of the specimens used.

Table 2 Specimen Details for Quasi-Steady State Experiments

| ASPECT RATIO | LENGTH | DIAMETER | WEIGHT |
|--------------|----------|----------|----------|
| 1 | 12.7mm | 12.7mm | 13.998gm |
| 3 | 38.1mm | 12.7mm | 41.37gm |
| 4 | 50.8mm | 12.7mm | 57.05gm |
| 8 | 50.8mm | 6.35mm | 14.45gm |
| 16 | 101.6mm | 6.35mm | 29.13gm |
| 24 | 152.4mm | 6.35mm | 44.36gm |
| 32 | 203.71mm | 6.35mm | 58.06gm |

To start the experiment, the immersion heaters were set at 80% of full rated value. With the onset of boiling, the hot and heavier FC5311® vapors rise, displacing air from the jar. The heater power and cooling water flow rate were adjusted so that the vapor/air interface was at the top of the condensing coils. This reduced the intermixing of air in the vapor zone and reduced turbulence at the air/vapor interface. The vapor temperature was constantly monitored to ensure saturated conditions inside the jar and the system was allowed to stabilize under saturated conditions for an hour and half. Temperature measurements were

started just as the specimen was lowered through the cover into position and continued until the specimen was in thermal equilibrium with the vapor. The specimen thermocouple was connected to a National Instruments data acquisition (DAQ) board (AT-MIO-16E10) through a signal conditioner. The specimen thermocouple voltage was sampled at a rate of 30~40Hz to enable accurate determination of $dT_w/d\tau$ at each measured specimen temperature T_w . The specimen temperature and temperature gradient profiles are shown in Fig. 3. When the specimen is inserted into the jar, transient condensation sets in forming a liquid film on the specimen. However, once the film is established, quasi-steady condensation occurs until the temperature of the specimen approaches T_{sat} asymptotically.

3. Analysis

The timed measurements of specimen and vapor temperatures are used to calculate $dT_w/d\tau$ and ΔT_w , where $dT_w/d\tau = \Delta T_w/\Delta\tau$, was calculated from the sequence of temperature measurements at every 4° rise in temperature of the specimen. The sphere surface temperature for each case was obtained directly from the measured temperature at that instant. The fluid properties were calculated at the mean film temperature T_m (Mahajan *et al.* 1991). The heat transfer coefficient h , at a measured specimen temperature, T_w , was determined using the lumped capacity relation,

$$m_c C_{pc} (dT_w/d\tau) = hA(T_{sat} - T_w) \quad (2)$$

where m_c , C_{pc} and A are the mass, specific heat and surface area of the specimen, respectively. The experimental Nusselt number $Nu_{exp} (= hD/k_l)$ was evaluated for each experiment; D being the characteristic length of the specimen. Since the Bi number ($= hD/k_c$), k_c being the thermal conductivity of copper, is less than 0.02 for all the specimens, the lumped capacity relation does not introduce significant error to the analysis.

For calculating the theoretical Nusselt number, it must be determined whether the experiment is truly quasi-steady. Furthermore, a relation between the quasi-steady and steady state calculations needs to be obtained. Using Dhir's (1975) quasi-steady results for steam condensation, Mahajan *et al.* (1991) have shown that quasi-steady approximations can be safely used for condensation on spheres for high Stefan number fluids since the ratio of local and steady state condensate film thickness was close to unity, to within 0.8%. Theoretical values for Nusselt number can be evaluated from the full boundary layer solutions of Sparrow and Greg (1959). However, for high Prandtl numbers (as in present case), these results can be closely approximated by calculations of Rohsenow (1956), even for high Stefan number fluids (see Mahajan *et al.* (1991)). In this paper, we follow their approach in calculating theoretical values of Nusselt numbers.

Horizontal Cylinder:

$$Nu_{th,h} = 0.728 \left[(\rho_l - \rho_v) g h'_{fg} D^3 / (v_l k_l \Delta T) \right]^{1/4} \quad (3a)$$

Vertical Cylinder:

$$Nu_{th,v} = 0.943 \left[(\rho_l - \rho_v) g h'_{fg} L^3 / (v_l k_l \Delta T) \right]^{1/4} \quad (3b)$$

As pointed out by Merte (1973), Eq. 3(b) is valid only if the diameter of the cylinder is much larger compared to the film thickness.

For horizontal and vertical cylinders of finite dimensions, the relations 3(a) and 3(b) are modified to obtain composite Nusselt numbers.

Horizontal cylinders:

$$Nu_{cal,h} = h_{cal,h} D / k_l \quad (4a)$$

where $h_{cal,h}$ is the area-averaged heat transfer coefficient of the different surfaces of the cylinder and D is the diameter of the cylinder. The heat transfer coefficient for the circular vertical sides of the horizontal cylinders was obtained by integrating Eq. 3(b) over the circular surface to give

$$h_{Sides} = 0.992 \left[(\rho_l - \rho_v) g h'_{fg} k^3 / (v_l \Delta T D) \right]^{1/4} \quad (4b)$$

Note that this coefficient is 5% higher than that of Eq. 3(b).

Vertical Cylinders:

$$Nu_{cal,v} = h_{cal,v} D / k_l \quad (5a)$$

where $h_{cal,v}$ is, again, the area-averaged heat transfer coefficient of the different surfaces of the cylinder, including the top, bottom and vertical side. For the top and the vertical surfaces, we follow the analysis by Bejan (1991) using the following correlations.

$$h_{Top} = 1.368 \left[(\rho_l - \rho_v) g h'_{fg} k^3 / (v_l \Delta T D) \right]^{1/5} \quad (5b)$$

$$h_v = 0.943 \Pi_L^{1/4} \left[(1 + B)^{3/4} - B^{3/4} \right] \quad (5c)$$

where L is the length of cylinder, $\Pi_L = h'_{fg} (\rho_l - \rho_v) L^3 / (k_l \Delta T v_l)$ and $B = 0.259 (D/L)^{4/5} \Pi_L^{-1/15}$. The heat transfer coefficient for the horizontal bottom of the vertical cylinders is based on fully developed Taylor instability and is calculated using correlation proposed by Gerstmann and Griffith (1967).

$$h_{Bottom} = 0.69 (Ra)^{0.20} \quad (5d)$$

where $Ra = \left[(g (\rho_l - \rho_v) h'_{fg} / (k_l \Delta T v_l)) (\sigma / [g (\rho_l - \rho_v)]) \right]^{3/2}$

In the theoretical correlations shown above, fluid properties are evaluated at T_m . However, for the fluids under consideration, significant property variations occur over the range of temperature differences encountered during the experiment. Hence, as pointed out by Mahajan *et al.* (1991), the power law correction factor based on viscosity ratio should be adopted to correct the theoretical Nusselt numbers. It was observed that the ratio of viscosities at the saturation and wall temperatures did a consistent job in correcting for large property variation during different sets of quasi-steady and steady state experiments.

$$Nu^* = Nu (\mu_{sat} / \mu_w)^{0.11} \quad (6)$$

4. Experimental Results and Discussions

We first carried out condensation experiments with spheres of diameter 12.5mm and 25.4mm to benchmark our setup. As in Mahajan *et al.* (1991), Nu_{exp} / Nu_{th}^* were plotted with Stefan number. The Nusselt ratio plotted in Fig. 4 shows a strong similarity with the results obtained by Mahajan *et al.* (1991).

FC5311[®] has a boiling temperature of 215°C at atmospheric pressure. As the sphere temperature rises during an experimental run, an increasing fraction of the vapor becomes noncondensables. In order to understand laminar film condensation on different geometries, it was necessary to account for the effect of noncondensables during condensation heat transfer with different specimens. The deterioration of heat transfer coefficient due to noncondensables obtained from these benchmarking experiments with spheres was, therefore, used to compensate the theoretical results for cylindrical specimens. The compensating polynomial is obtained as a function of Stefan number by fitting a trend line to the Nusselt ratio plot for sphere, as shown in Fig. 4.

$$\Phi(S) = 4.2107 \times 10^{-2} S^3 - 1.5818 \times 10^{-1} S^2 + 2.3327 \times 10^{-1} S + 6.0408 \times 10^{-1} \quad (7)$$

where S varies between 0.5 to 3. In rest of the paper, we will use Eq. (7) in conjunction with our experimental data to compensate for the effect of non-condensables

4.1. Horizontal Cylinders

Figure 5 shows a typical plot of the heat transfer coefficients for a horizontal cylinder with aspect ratio unity. At the beginning of the experiment ΔT is high and h is low. As the wall temperature rises, the heat transfer coefficient also rises. Before applying laminar film condensation theory to the experimental data, it was necessary to determine the nature of the flow regime of the condensate film. To this end, the liquid Reynolds number was evaluated at every measured temperature from Eq. (2) and plotted against respective Stefan number.

$$\text{Re}_L = \frac{4\Gamma}{\mu} = \frac{4}{\mu} (h\Delta T(\pi D)/h_{fg}) \quad (8)$$

where μ denotes dynamic viscosity of the condensate. The plot is shown in Fig. 6. Based on the capillary-gravitational linear scale, the straight line on the graph represents the transition of the liquid-vapor interface from laminar smooth to laminar wavy for falling film condensation Brauer (1956).

$$\text{Re}_L = 9.3Ar^{1/5} \quad (9a)$$

where $Ar = [g/\nu^2 \{ \sigma / \{ g(\rho_l - \rho_v) \} \}]^{3/2}$ and σ is the surface tension of the condensate. The transition from laminar-wavy film to turbulent-wavy film (Kutateladze, 1982) is given by:

$$\text{Re}_L = 35Ar^{1/5} \quad (9b)$$

The graph reveals that the specimens with higher aspect ratios have a smooth laminar film. The only specimen, on which the condensate film comes close to becoming laminar wavy at a certain Stefan number, is the one with smallest aspect ratio ($\alpha=1$). Therefore, the theoretical relations discussed in previous section can be safely used to compare experimental Nusselt numbers.

Next, we plot the results of the quasi-steady experiments with horizontal cylinders for different aspect ratios ($\alpha=L/D$) in Fig. 7. The ratio $Nu_{\text{exp}}/Nu_{\text{th},h}^*$ for horizontal cylinders is plotted against the Stefan number. The Nusselt ratio for a given Stefan number is higher at low aspect ratios. This is due to increased contribution of heat transfer from the vertical sides. Moreover, cross flow of condensate from the horizontal surface to the vertical surface decreases the thickness of the condensate layer on the cylindrical surface and hence, increases overall heat transfer from the specimen. The extent of cross flow on high aspect ratio specimens is low. As expected, the average heat transfer from the specimen decreases as the aspect ratio increases.

To understand the contribution of cross flow on film condensation, we compare the normalized experimental Nusselt ratio $(Nu_{\text{exp}}/Nu_{\text{th},h}^*)/\Phi(S)$ with that based on composite Nusselt number (Eq.(4a)). The experimental data is divided by $\Phi(S)$ to eliminate the non condensable effect for comparison purposes. The experimental data for each specimen is plotted in Fig.8 for three different values of Stefan number. We note that for low aspect ratio specimens, the experimental Nusselt ratios are consistently higher than the analytical values over the range of Stefan numbers. High cross flow thins the condensate film and decreases the thermal resistance of the film. However, with a rise in aspect ratio, the amount of cross flow decreases and the relative heat transfer contribution of vertical sides drops. Now the retention of condensate on the cylinder surface is only determined by the surface tension forces in the film and the weight of the condensate accumulated on the cylinder. The thickening of the condensate layer due to individual drop growth spreads over a larger part of the cylinder surface than that predicted by Nusselt. The condensate flow on the cylinder

surface is reduced, thus, increasing the film thickness and decreasing the heat transfer below values predicted by Nusselt-Rohsenow theory. To account for this deterioration, Colburn and Hougen (1930) have suggested using 0.6072 instead of 0.728 in the relation for $Nu_{th,h}$ (Eq.3(a)). The plot of $(Nu_{cal,h})_{\sigma} / Nu_{th,h}$ reflects this modification in Fig.8.

The experimental Nusselt ratio plotted in Fig.8 can now be used to formulate a correlation, which also takes care of the surface tension effects.

$$Nu_{Exp} / (Nu_{th,h})_{\sigma} = 1 + 0.41\alpha^{-0.42} \quad \text{where } \alpha \geq 1 \quad (10)$$

where $\alpha(=L/D)$ denotes aspect ratio of specimen and $(Nu_{th,h})_{\sigma}$ represents the theoretical Nusselt number for condensation on horizontal tubes corrected for surface tension effects (Colburn and Hougen, 1930). For high aspect ratios, the second term on RHS is negligible and, hence, the ratio approaches unity. The present correlation however, needs further improvement to be used for low aspect ratio ($\alpha < 1$) specimens. The high Nusselt ratios for $\alpha=24$ and 32 at $S=1.5$ are due to experimental uncertainties introduced by convection during insertion of specimens

4.2. Vertical Cylinders

Figure 9 shows the plot of liquid Reynolds number against Stefan numbers. The Stefan numbers represent different quasi-steady states of condensation. The Re_L plot shows that specimens with aspect ratio greater than 8 have a laminar-wavy condensate film.

The plot of Nusselt ratio against Stefan number in Fig. 10 indicates that condensation heat transfer is higher for specimens with high aspect ratio. This is primarily because of increased contribution from the high heat transfer at the vertical surface and decreased contribution from the low heat transfer from the top and bottom surfaces of the cylinder.

Figure 11 shows the deviation of condensation heat transfer from theoretical predictions as a function of aspect ratio of the specimen for different Stefan numbers. While $Nu_{th,v}$ is evaluated based on the Nusselt-Rohsenow correlation for a vertical surface modified by Bejan (1991), $Nu_{th,h}$ has area-weighted contributions from the top, bottom and vertical surfaces of the specimen. The theoretical predictions are represented by an empirical correlation.

$$Nu_{cal,v} / Nu_{th,v} = 1 - 0.27e^{-0.54\alpha} \quad \text{where } \alpha \geq 1 \quad (11)$$

For the purpose of comparison, experimental values are modified for thermal resistance due to noncondensables by the term $\Phi(S)$. Condensation on the horizontal top surface affects total rate of condensation on the specimen in two ways. It contributes directly through the heat transfer from the surface and indirectly by thickening the condensate film that coats the vertical surface. At low aspect ratio, heat transfer from the specimen is dominated by the condensate inundating from the top surface. The condensate draining from the top of the specimen indirectly increases thermal resistance on the vertical surface by thickening the film. This explains the deficit in experimental values for specimens with $\alpha < 8$. At higher aspect ratios, the heat transfer contribution from the top surface is reduced and so is the condensate inundating from the top surface. The increased length of the specimen provides surface for the condensate film interface to develop and transit from smooth-laminar to wavy-laminar. The onset of waviness on the vertical surface increases the heat transfer from the specimen above the theoretical predictions.

5. Summary

In the present study the horizontal cylinder results indicate that for large aspect ratios (>16) condensation heat transfer coefficients were close to those predicted by Nusselt-

Rohsenow correlation for horizontal cylinders. With decrease in aspect ratio, the heat transfer rate increased due to

- Increasing contribution from the high heat transfer at the vertical surfaces
- Increased heat transfer at the surface due to thinning of condensate film caused by cross flow

For vertical cylinders, condensation heat transfer for high aspect ratio (>8) was higher than that predicted by vertical plate Nusselt correlation. However, temperature measurements also indicated that condensation heat transfer from low aspect ratio specimens was below the theoretical predictions. Change in aspect ratio affected condensation heat transfer by

- Altering the direct and indirect contribution of the low heat transfer surface at the top and bottom of the specimen.
- Altering the onset of waviness in the condensate film.

6. References

- Bejan, A., 1991, "Film condensation on an upward facing plate with free edges", *Intl. J. Heat Mass Transfer*, Vol. 34, No. 2, pp578-582
- Brauer, H., 1956, "Strömung und Wärmeübergang bei Reiselfilmen", *VDI Forschung*, Vol. 22, pp1-40.
- Bromley, L. A., Brodkey, R. S. and Fishman, N., Dec 1952, "Heat transfer in condensation: Effect of Temperature variation around a horizontal condenser tube", *Ind. Eng. Chemistry*, Vol. 44, No. 12, pp2962-2966
- Bromley, L. A., Dec 1956, Heat transfer in condensation: Effect of heat capacity of condensate" *Ind. Eng. Chemistry*, Vol. 44, No. 12, pp2966-2969
- Chen, M. M., Feb 1961, "An analytical study of laminar film condensation: Part 1-Flat Plates", *ASME J. Heat Transfer*, Vol. 83, pp48-54.
- Chen, M. M., Feb 1961, "An analytical study of laminar film condensation: Part 2-Single and Multiple Horizontal Tubes", *ASME J. Heat Transfer*, Vol. 83, pp55-60
- Colburn, A. P. and Hougen, O. A., 1930, "Studies in Heat Transmission. II Dehumidification", *Ind. Eng. Chem.*, Vol. 22, pp 525.
- Dhir, V. K., Aug 1975, "Quasi-Steady laminar film condensation of steam on copper spheres", *J. Heat Transfer*, Vol. 97, p 347-351
- Dhir, V. K. and Leinhard, J. H., Feb 1971, "Laminar film condensation on plane and axi-symmetric bodies in non-uniform gravity", *J. Heat Transfer*, Vol. 95, No.1, p97-100
- Gerstmann, J. and Griffith, P., 1967, "Laminar film condensation on the underside of horizontal and inclined surfaces", *Intl. J. Heat Mass Transfer*, Vol. 10, pp567-580
- Koh, J. C. Y., Sparrow, E. M. and Hartnett, J. P., 1961, "The two phase boundary layer in laminar film condensation", *Intl. J. Heat Mass Transfer*, Vol. 2, p. 69
- Kutateladze, S. S., 1982, "Semi-Empirical theory of film condensation of pure vapors", *Intl. J. Heat Mass Transfer*, Vol. 25, No. 5, pp653-660
- Leppert, G. and Nimmo, B., Feb 1968, "Laminar film condensation on surfaces normal to body or inertial forces", *Trans. ASME*, Vol. 90, p 178-179
- Mahajan, R. L., Chu, T. Y. and Dickinson, D. A., May 1991, "An experimental study of laminar film condensation with Stefan number greater than unity", *ASME J. Heat Transfer*, Vol. 113, pp472-478.
- Merte, H., Jr., 1973, "Condensation heat transfer", *Advances in Heat Transfer*, Vol. 9, p181, Academic Press
- Rohsenow, W. M., Nov 1956, "Heat transfer and temperature distribution in laminar film condensation", *Trans. ASME*, Vol. 78, p1645-1648
- Rose, J.W., Feb 1998, "Condensation heat transfer fundamentals", *Trans. IChemE*, Vol. 76, Part A, pp143-152.
- Selin, G., Aug. 1961, "Heat transfer by condensing pure vapors outside inclined tubes", *Proc. Intl. Heat Transfer Conf.*, Part II, pp279-289
- Shigechi, T., Kawae, N., Tokita, Y. and Yamada, T., 1993, "Film condensation heat transfer on a finite size horizontal plate facing upwards", *Heat Transfer-Japanese Research*, Vol.22, No. 1, pp66-77
- Sparrow, E. M. and Siegel, R., Mar 1959, "Transient film condensation", *ASME J. Applied Mechanics*, Vol. 81, No. 1, p. 120.

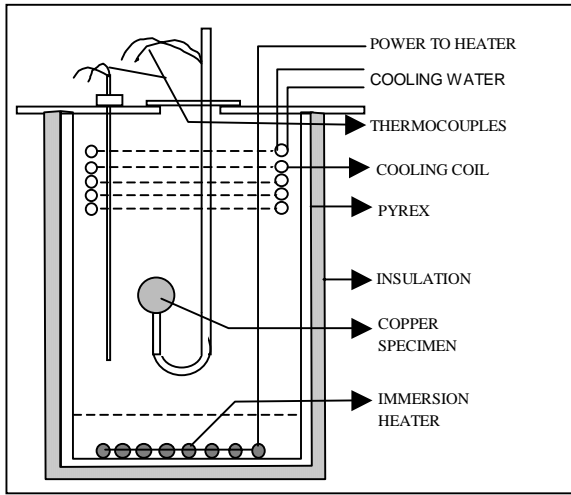


Fig.1 Schematic of the Experimental Setup

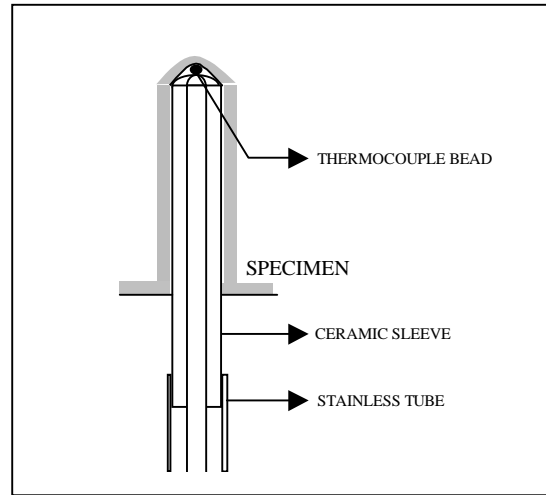
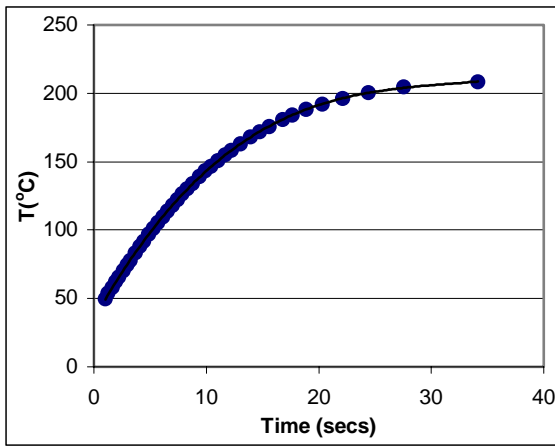
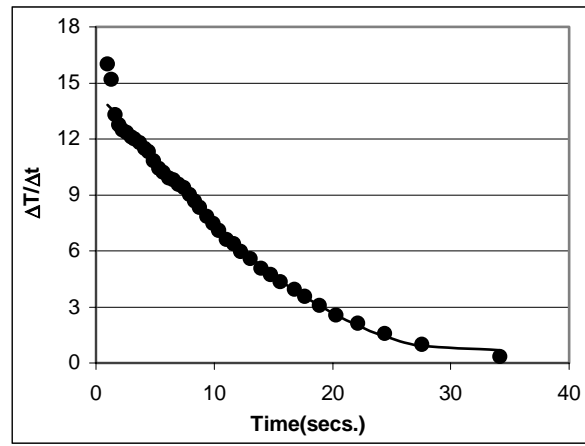


Fig. 2 Detail of thermocouple attachment to specimen



Temperature Vs Time



Rate of Temperature rise Vs Time

Fig.3 Temperature and Rate of change of Temperature with Time

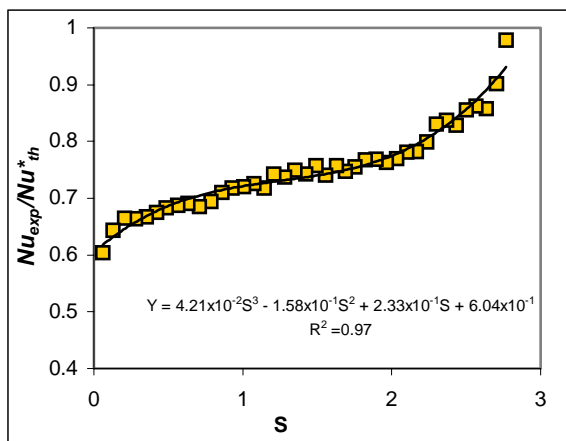


Fig.4 Condensation heat transfer on spheres

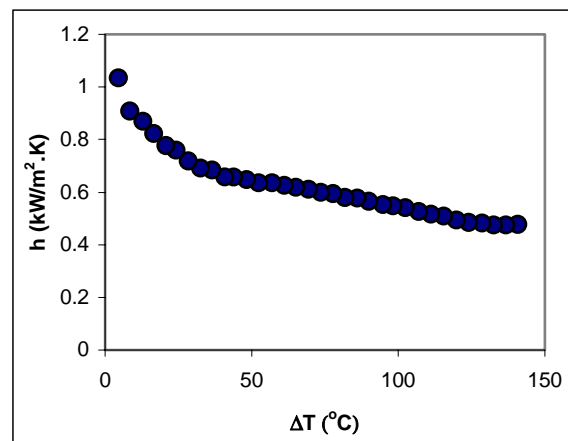


Fig.5 Condensation heat transfer coefficients ($\alpha=1$)

